Mineralogical Magazine (2021), **85**, 364–378
doi:10.1180/mgm.2021.29

CAMBRIDGE UNIVERSITY PRESS

Article

In situ trace elements and S isotope systematics for growth zoning in sphalerite from MVT deposits: A case study of Nayongzhi, South China

Chen Wei[1,2], Lin Ye[1]*, Zhilong Huang[1], Yusi Hu[1,2]* and Haoyu Wang[1,2]

[1]State Key Laboratory of Ore Deposit Geochemistry, Institute of Geochemistry, Chinese Academy of Sciences, Guiyang 550081, China; and [2]University of Chinese Academy of Sciences, Beijing, 100049, China

Abstract

Zoning texture in sphalerite has been described in many studies, although its genesis and ore formation process are poorly constrained. In this investigation, we compare the *in situ* trace element and isotopic composition of colour-zoned sphalerites from Nayongzhi, South China, to explain the zoning growth process. Petrographic observations identified two broad types of zoned sphalerite, core–rim (CR) and core–mantle–rim (CMR) textures. Each zoned sphalerite displays two or three colour zones, including brown core, light colour bands and/or pale-yellow zones. *In situ* laser ablation inductively coupled plasma mass spectrometry trace-element analyses show that the three colour zones display variable trace-element compositions. Brown cores exhibit distinctly high Mn, Fe, Co, Ge, Tl and Pb concentrations, whereas pale-yellow and light colour zones have elevated Ga, Cd, Sn, In and Sb concentrations. Copper, Sb, In and Sn show slight variations between pale-yellow and light zones, the latter having higher In and Sn, but lower Cu and Sb abundances. Given the low concentration range of Pb, Ge, Tl, Mn Sb, Cd, etc., the colour of sphalerite is attributed mainly to Fe compositional variation. The $\delta^{34}S$ values of sphalerite from Nayongzhi range from +22.3 to +27.9‰, suggesting reduced sulfur was generated by thermochemical sulfate reduction of marine sulfate in ore-hosted strata. Single-crystal colour-zoned sphalerite exhibits intracrystalline $\delta^{34}S$ variation (up to 4.3‰), which is attributed to the $\delta^{34}S$ composition of H_2S in the original fluid. The lack of correlation between trace elements and $\delta^{34}S$ values indicates episodic ore solution influxes and mixes with the reduced sulfur-rich fluid derived from the aquifers of the ore-hosted strata, which play a key role in the formation of the zoned Nayongzhi sphalerite. In conclusion, *in situ* trace element and S isotope studies of zoned sphalerite crystals might provide insight into the ore-forming process of MVT deposits.

Keywords: sphalerite, LA-(MC)-ICP-MS, trace elements, *in situ* S isotope, TEM, growth mechanism

(Received 20 October 2020; accepted 22 March 2021; Accepted Manuscript published online: 26 March 2021; Associate Editor: Jason Harvey)

Introduction

Sphalerite (ZnS) is a common mineral in sulfide deposits, and the bulk of Zn and critical elements such as Ge, Ga, In, etc. are extracted from sphalerite ore (Höll *et al.*, 2007; Cook *et al.*, 2009, 2011; Frenzel *et al.*, 2017 and reference therein). The mineral occurs in diverse textures such as euhedral crystals, concentric zoning and colloform textures (McLimans *et al.*, 1980; Pattrick *et al.*, 1993; Barrie *et al.*, 2009). These textures, common in various types of Ag–Pb–Zn and Au–Ag veins and in Mississippi Valley-type (MVT) deposits (Barton *et al.*, 1977; Di Benedetto *et al.*, 2005; Barrie *et al.*, 2009; Belissont *et al.*, 2014), record physicochemical conditions during mineral formation (Pattrick *et al.*, 1993), and illustrate the sequential evolution of hydrothermal fluids (e.g. Kelley *et al.*, 2004).

Zoning textures in sphalerite have been described in most studies of the metallogeny of Zn–Pb deposits but very few investigations have examined the causes of the zoning. There are a few notable exceptions (Roedder, 1968; McLimans *et al.*, 1980; Pattrick *et al.*, 1993; Di Benedetto *et al.*, 2005; Pfaff *et al.*, 2011 and Gagnevin *et al.*, 2012). The pioneering work of Roedder and Dwornik (1968) showed the total Fe content varies between bands but does not display any correlation with the colour of the band. In contrast, McLimans *et al.* (1980) considered that the colour of the bands is related to the FeS content due to a strong relationship between colour and iron content. Pattrick *et al.* (1993) proposed that repetitive bands are associated with cyclic changes in solution pH. Recently, Gagnevin *et al.* (2012) proposed that layered sphalerite in Irish-type deposits forms by mixing two compositionally and isotopically contrasting hydrothermal fluids. Older publications have mostly relied on electron microprobe (EMP), scanning electron microscopy (SEM) and/or wet chemistry. However, the utility of EMP is restricted because of the relatively high detection limits (mostly >100 ppm). Although wet chemistry can provide quantitative results for trace elements and isotopes, the micro-scale chemical

***Authors for correspondence:** Lin Ye, Email: yelin@vip.gyig.ac.cn; Yusi Hu, Email: huyusi@mail.gyig.ac.cn

Cite this article: Wei C., Ye L., Huang Z., Hu Y. and Wang H. (2021) *In situ* trace elements and S isotope systematics for growth zoning in sphalerite from MVT deposits: A case study of Nayongzhi, South China. *Mineralogical Magazine* **85**, 364–378. https://doi.org/10.1180/mgm.2021.29

and isotopic resolution is limited. This has resulted in limited documentation and understanding of the growth mechanism of zoned sphalerite—limiting its utility in reconstructing the evolution of hydrothermal fluids. Recent advances of *in situ* microanalytical techniques such as laser ablation inductively coupled plasma mass spectrometry (LA-ICP-MS) and secondary ion mass spectrometer (SIMS) can provide, not only the quantitative results for trace elements present at very low concentrations (~0.01 ppm; Cook *et al.*, 2009), but also offers an attractive option for qualitative mapping of low concentrations of trace elements at high spatial resolution (Large *et al.*, 2009). Furthermore, LA-Multi-Collector-ICP-MS (LA-MC-ICP-MS), with a spot size as small as 20 μm, provides an opportunity to study sulfur isotope composition of individual growth bands of minerals (Pfaff *et al.*, 2011).

In this investigation, we present detailed observations of growth zones in sphalerite from vein-hosted sphalerite from the Nayongzhi MVT Zn–Pb deposit, South China. *In situ* LA-ICP-MS trace-element spot analyses, element-distribution maps and LA-MC-ICP-MS sulfur isotope analyses were used to: (1) reveal the relationship between colour and trace elements in sphalerite; (2) constrain the sulfur isotope variation on a crystal scale; and (3) determine the possible control factors on the formation of zoned sphalerite. Finally, a possible growth process to explain the observed zoned sphalerite is proposed.

Geology of the Nayongzhi MVT deposit

The Nayongzhi MVT deposit is located at the eastern border of the Sichuan–Yunnan–Guizhou metallogenic province, on the southwestern edge of the Yangtze Platform (Fig. 1a,b). The deposit lies in the NE-trending Wuzhishan anticline and is limited by two parallel NNE-trending regional faults, the Jichangpo and the Xiongchang faults (Fig. 1c; Wei *et al.*, 2018a and reference therein). In the Nayongzhi area, the lower Cambrian Qingxudong Formation is divided into three members based on lithological features: (1) argillaceous dolostone and carbonaceous dolostone; (2) laminated dolostone interlayered with zebra dolostone; and (3) fine-grained dolostone and argillaceous dolostone (e.g. Jin *et al.*, 2016). The orebodies are hosted primarily in the junction between the members 1–2 of the Qingxudong Formation and consist of two principal types, a stacked series of stratabound lenses and steeply dipping veins with the stratabound lenses primarily in the Qingxudong Formation and the steeply dipping veins within the F_{12} fault (Fig. 1d). The Zn–Pb ore is associated spatially and temporally with the NW-trending F_{12} thrust fault. High-grade orebodies occur mainly as massive solution-collapse breccias and veins in proximity to the F_{12} fault, however, low-grade replacement orebodies mainly occur as stratiform and/or lentiform bodies far from the F_{12} fault, suggesting the F_{12} fault probably acted as an efficient conduit for an upward flowing hydrothermal fluid (Wei *et al.*, 2020).

The economic minerals in the Nayongzhi MVT deposit consist of sphalerite and galena with minor pyrite, accompanied by hydrothermal dolomite and calcite as the main gangue minerals. The main ore stage consists of coarsely crystallised sphalerite and galena, accompanied by fine-grained pyrite with co-existing hydrothermal dolomite (Wei *et al.*, 2018a; Zhou *et al.*, 2018). Coarsely crystallised sphalerite is essentially restricted to cavity and fracture fillings of the host rock (Wei, 2018), which is a common texture of the main ore stage.

Sampling and analytical methods

Sampling

Four representative sphalerite ore samples (16L-10, 16L-9-1, 16S-35 and 16S-36) were collected from different sulfide veins (0.2–1 m wide) in the underground tunnels of level 1270 m and 1290 m, respectively. Specifically, samples (16L-10 and 16L-9-1) were collected from the proximity of the F_{12} fault, whereas samples 16S-35 and 16S-36 were collected from ~2.2 km away from the F_{12} fault. Detailed sampling locations are shown in Fig. 1c–d.

LA-ICP-MS multi-element analysis and element mapping

Spot analysis using LA-ICP-MS and element-distribution maps were acquired at the State Key Laboratory of Ore Deposit Geochemistry, Institute of Geochemistry Chinese Academy of Sciences (IGCAS), using a high-performance RESOlution 193nm ArF excimer Laser Ablation System coupled to an Agilent 7700x ICP-MS instrument. The ablated aerosol transported using a constant He (350 ml/min) flow and mixed with Ar (900 ml/min) in a cyclone coaxial mixer before entering the ICP-MS. Spot ablation was carried out using a 26 μm spot size at ~3 J/cm^2 with a 5 Hz pulse frequency. Each analysis incorporated a background acquisition of ~30 s (gas blank) followed by 60 s of data acquisition from the sample. The following isotopes were monitored: ^{23}Na, ^{27}Al, ^{29}Si, ^{34}S, ^{49}Ti, ^{51}V, ^{55}Mn, ^{57}Fe, ^{59}Co, ^{60}Ni, ^{65}Cu, ^{66}Zn, ^{72}Ge, ^{75}As, ^{85}Rb, ^{88}Sr, ^{107}Ag, ^{111}Cd, ^{115}In, ^{118}Sn, ^{121}Sb, ^{205}Tl and ^{208}Pb. Internal calibration used ^{66}Zn, with the measured 64.6 wt.% data from EMP analyses (Wei *et al.*, 2018a). External reference materials STDGL2b3 (Danyushevsky *et al.*, 2011), GSD-1G and GSE-1G were used for instrument drift correction and trace-element quantification. These were run before analyses of the unknown samples and after every 1.5 h to record instrumental drift. Data reduction calculations and error propagations were performed using *LADR* software designed at the analytical laboratories of the Centre of Excellence in Ore Deposits (CODES), University of Tasmania, following the standard methods of Longerich *et al.* (1996). The complete trace-element dataset for each element in each sample are given in the Supplementary material (see below).

Element maps were obtained by ablating sets of parallel lines across the sphalerite using a consistent laser spot size (9 μm) and 10 μm/s scan speed at a laser repetition of 10 Hz and 0.002 s dwell time for all measured elements. Identical rasters were done on the reference material of STDGL2b3, GSE-1G and GSD-1G at the start and end of a mapping run to calculate element concentrations in sphalerite and to correct for instrumental drift. Element maps were compiled and processed using the program *Iolite* (Paton *et al.*, 2011) and an add-in for the data analysis program *Igor* developed by WaveMetrics. All LA-ICP-MS maps were produced for each element using a logarithmic colour scale.

LA-MC-ICP-MS sulfur analysis

In order to study the sulfur isotopes with respect to colour-zoned sphalerite, polished thin sections used for LA-ICP-MS trace element spot analysis were repolished and used for *in situ* sulfur isotope analysis. *In situ* sulfur isotopes were measured using a Nu-Plasma 1700 multicollector ICP-MS (Nu Instruments, United Kingdom) at the State Key Laboratory of Continental

https://doi.org/10.1180/mgm.2021.29 Published online by Cambridge University Press

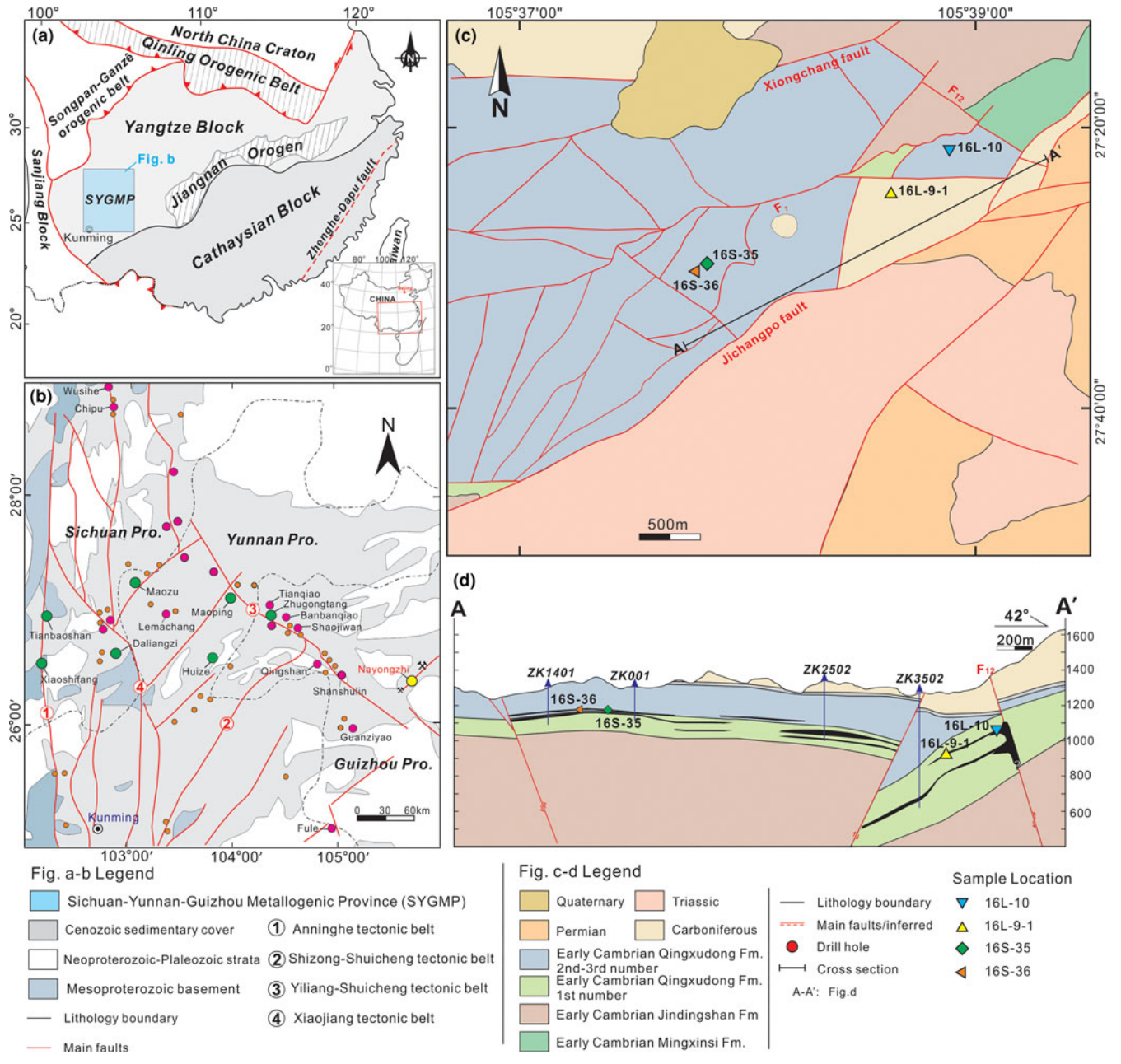

Fig. 1 (a) The location of the Sichuan–Yunnan–Guizhou metallogenic province (SYGMP) in South China (modified from Wei *et al.*, 2018a); (b) location of the Nayongzhi deposit in the SYGMP (modified from CIGMR, 2003); (c) simplified geological map of the Nayongzhi deposit; (d) representative cross-section showing the occurrence and morphology of the sulfide orebodies at Nayongzhi. The location of the section is indicated in (c).

Dynamics (SKLCD), Northwest University, China. Sphalerite samples were ablated at a spot size of 30 μm, using a fluence of 3.6 J/cm^2 at 3 Hz. The total S signal obtained for sphalerite was typically 8 to 12 V. Under these conditions, after a 30 s baseline, 50 s of ablation is needed to obtain an internal precision of $^{34}S/^{32}S \leq \pm 0.000002$ (1σ). More details of the method can be found in Chen *et al.* (2017). Two in-house standards were used for external standard bracketing (NWU-Py-4) and quality control (PTST-2) of analyses (Chen *et al.*, 2017). The $\delta^{34}S_{CDT}$ (‰) of PTST-2 yielded in this investigation were 32.4±0.4‰ (2σ, $n = 35$), which agree well with that of the reported value of 32.5±0.3‰ (2σ) measured by gas source-mass spectrometry or solution-introduced MC-ICP-MS (Chen *et al.*, 2017).

Focused ion beam and transmission electron microscopy study

Two thin foils for transmission electron microscopy (TEM) investigation were prepared using a Dual-Beam focused ion beam (FIB) system (FEI Helios Nanlab 350S) at the Center for Lunar and Planetary Sciences, IGCAS. For this investigation, foils with a size of 15 μm × 15 μm × 0.1 μm at chosen locations within sphalerite were sputtered with Ga ions accelerated to 30 keV. Each foil was placed on a copper grid and thinned. TEM characterisation was performed using an FEI Tecnai G2 F20 S-TWIN TEM system at the State Key Laboratory of Environmental Geochemistry, IGCAS. The TEM is equipped with an energy-dispersive X-ray spectrometer (EDAX) and high angle annular dark field (HAADF) detector in STEM mode.

https://doi.org/10.1180/mgm.2021.29 Published online by Cambridge University Press

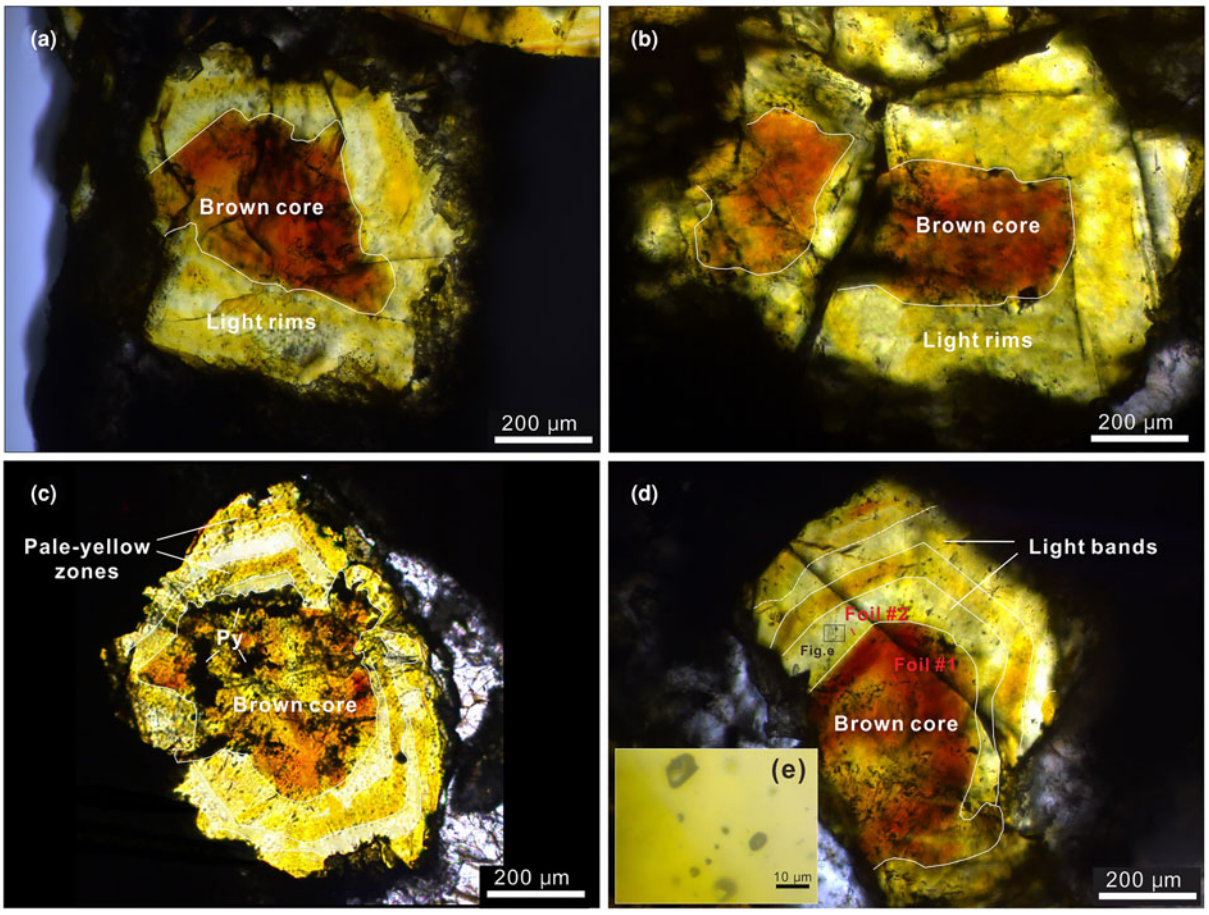

Fig. 2. Transmitted light microphotographs of the zoned sphalerite from Nayongzhi showing the main zoning patterns: (a) Sample 16S-35; (b) sample 16S-36; (c) sample 16L-9-1; (d) sample 16L-10; and (e) magnified insert showing inclusions.

Results

Petrography

Optical microscope observations of the analysed sphalerite samples show obvious core–rim (CR) zonation (Fig. 2). Minor inclusions of galena and pyrite can be observed in sphalerite from sample 16L-10 (Fig. 2c). The thickness of discrete zones varies between 80 μm and 500 μm (Fig. 2). Colour variations in CR zoned sphalerite are dramatic, with brown zones contrasting with pale-yellow and/or light zones, with a cross-section width of no more than 100 μm (Fig. 2). Sphalerite grain size varies significantly within the samples and individual sphalerite crystals can have up to five discrete colour zones. Cursory observations suggest two typical optical colour zoning patterns in sphalerite crystals: (1) CR texture (Fig. 2a,b) and (2) core–mantle–rim (CMR) texture (Fig. 2c,d). Specifically, CR texture, generally coarse grained (~1 mm), occurs as a brown core (200–400 μm) and light rim with highly variable width (Fig. 2a,b) and were observed in samples 16S-35 and 16S-36 (the distal part of the F_{12} fault; Fig. 1c,d). Whereas the CMR texture includes a brown core (300–500 μm) and alternate parallel pale-yellow and light growth bands that vary in thickness from 60 μm to 150 μm; this appears flattened (Fig. 2c,d) and is common in samples 16L-10 and 16L-9-1, collected from proximal to the F_{12} fault (Fig. 1c,d). Notably, many fluid inclusions were observed in all three colour zones within these sphalerite (Fig. 2e).

Trace-element compositions

All analytical data for minor and trace elements in sphalerite determined by LA-ICP-MS are presented as Supplementary material and summarised in Table 1. LA-ICP-MS ablation profiles were generally smooth, suggesting homogeneous distribution of elements in the spot analysed (Fig. 3). No discrete nanoparticles were detected by TEM in any of the analysed foils suggesting homogeneous incorporation of trace elements into the sphalerite lattice (Fig. 4 a,b). A fluid inclusion, 80 nm diameter, in the brown sphalerite zone (foil #2) was observed by TEM (Fig. 4c). Line scans with EDAX indicate an area of 50–70 nm in width with increasing Ge, Co, Fe, Cl, Si and Pb concentrations and simultaneously decreasing Zn and S values (Fig. 4d).

Comparative boxplots of minor and trace elements in the three identified colour zones of sphalerite are shown in Fig. 5, consisting of 42 spot analyses in brown cores, 26 spot analyses in pale-yellow bands and 45 spot analyses in light zones. Median values are used for comparison (Fig. 5).

Iron is the most abundant trace element in sphalerite with concentrations ranging between 0.11 and 2.34 wt.%. Highest concentrations can be found in brown cores, with a median value of 1.14 wt.%. Cadmium is the second most abundant trace element in the sphalerite sample analysed. The concentration of Cd varies from 189 to 2149 ppm, and is greatest in light zones, with a median value of 1350 ppm. Lead, Ge, Ga, Cu and Sb display highly variable

https://doi.org/10.1180/mgm.2021.29 Published online by Cambridge University Press

Table 1 LA-ICP-MS data for the three colour zones of sphalerite from the Nayongzhi Zn–Pb deposit.

		Mn	Fe	Co	Cu	Ga	Ge	As	Ag	Cd	In	Sn	Sb	Tl	Pb
Brown cores	Count	42	42	42	42	42	42	26	42	42	16	34	42	42	42
	Max	17.4	2.34	0.78	248	25.7	868	1.30	2.96	507	0.06	1.45	16.8	34.9	1733
	Min	8.21	0.38	0.25	31.3	0.25	306	0.34	0.75	189	0.01	0.04	1.38	10.3	354
	Median	13.1	1.14	0.48	73.2	1.48	557	0.67	1.87	317	0.02	0.20	3.40	19.7	631
	Mean	13.4	1.20	0.48	86.0	2.60	547	0.71	1.89	329	0.02	0.28	3.85	19.6	692
	S.D.	2.14	0.45	0.14	50.6	4.08	129	0.22	0.50	78.0	0.01	0.29	2.94	5.94	301
Pale-yellow bands	Count	26	26	26	26	26	26	19	26	26	26	26	26	26	26
	Max	12.2	0.82	0.41	309	285	551	3.54	4.76	1757	1.20	42.9	169	22.1	636
	Min	0.29	0.14	0.08	32.8	14.4	34.4	0.37	1.22	404	0.02	2.02	0.26	0.38	9.45
	Median	4.32	0.31	0.14	126	105	105	1.42	1.71	965	0.11	10.7	50.4	1.55	89.6
	Mean	5.51	0.35	0.18	130	113	161	1.63	1.94	1030	0.23	13.2	57.7	3.90	155
	S.D.	3.50	0.17	0.09	66.0	70.3	144	0.94	0.85	379	0.27	10.1	42.6	5.68	152
Light zones	Count	45	45	45	45	45	45	45	44	45	42	45	45	45	45
	Max	9.76	0.44	0.17	221	342	192	6.28	2.29	2150	0.46	24.4	206	3.96	176
	Min	0.54	0.11	0.04	26.8	7.85	4.25	0.64	0.89	594	0.01	0.14	30.5	0.05	25.3
	Median	1.83	0.20	0.11	113	185	27.2	1.80	1.48	1350	0.07	9.86	73.6	0.32	69.8
	Mean	2.23	0.21	0.11	122	186	38.8	2.08	1.52	1350	0.09	10.3	88.6	0.50	78.6
	S.D.	1.75	0.55	0.03	50.4	84.5	36.7	1.24	0.29	250	0.08	5.58	46.6	0.71	35.3

Note: Fe in wt.% and other elements in ppm

concentrations. These elements vary from 9.45–1733 ppm (median of 324 ppm), 4.25–868 ppm (median of 256 ppm), 0.25–342 ppm (median of 101 ppm), 26.8–309 ppm (median of 110 ppm) and 0.26–206 ppm (median of 50 ppm), respectively. Gallium, Cu and Sb are mostly concentrated in light zones, ranging from 7.85–342 ppm (median of 186 ppm), 32.8–309 ppm (median of 130 ppm) and 30.5–206 ppm (median of 88.6 ppm), respectively. Lead and Ge, however, are enriched in brown core zones, ranging from 354–1733 ppm (median of 692 ppm) and 306–868 ppm (median of 547 ppm), respectively. In addition, Mn, Tl and Co exhibit a wide range of concentrations (0.29–17.4 ppm, 0.05–34.9 ppm and 0.04–0.78 ppm, respectively) and are more concentrated in brown cores with median values of 13.4 ppm, 19.6 ppm and 0.48 ppm, respectively. Sliver, In and Sn extend from below the limit of detection to 4.63 ppm, 1.20 ppm and 42.9 ppm, respectively and are more enriched in pale-yellow bands. Further, As was detected in several spots, with concentrations ranging from below the limit of detection to 6.28 ppm (median of 1.59 ppm), with higher concentrations in light zones, with a median value of 2.08 ppm.

Trace-element distribution in zoned sphalerite

A typical optical colour CR pattern in single sphalerite crystals (~600 μm across) was chosen for LA-ICP-MS mapping (Fig. 6). Although the distribution of most analysed trace elements is heterogeneous, the element-distribution maps reveal two distinct compositional zoning patterns. Iron, Ge, Tl, Mn, Co, Pb and Ag are mainly concentrated in brown cores and depleted in ~200 μm wide light rims (Fig. 6). In contrast, light zones are preferentially enriched in Cd, Ga, Sb, In and Sn, relative to brown cores (Fig. 6).

The CMR pattern in sphalerite samples was not analysed by LA-ICP-MS elemental mapping due to the high abundance of fluid inclusions. Two linear traverses across the CMR texture of sphalerite from sample 16L-9-1 were acquired (Fig. 7). The traverses reveal that brown cores exhibit distinctly higher Mn, Fe, Co, Ge, Tl and Pb concentrations than pale-yellow and light zones (Fig. 7). However, pale-yellow and light zones have elevated Ga, Cd, Sn, In and Sb concentrations relative to brown cores (Fig. 7). These partition trends are comparable to what can be seen in the LA-ICP-MS elemental maps of CR patterns (Fig. 6). The concentration of trace elements such as Cu, Sb, In and Sn shows slight variation between pale-yellow and light zones (Fig. 7). Light zones have higher In and Sn but lower Cu and Sb abundances relative to the pale-yellow zones.

Sulfur isotopic compositions

The sulfur isotopic compositions were determined by *in situ* LA-MC-ICP-MS analyses (Table 2 and Fig. 8). All 20 spots correspond with prior trace-element spot analyses. The $\delta^{34}S$ values of seven spots in brown cores vary from +26.3 to +27.9‰, (mean of +27.4±0.7‰); five analyses of pale-yellow bands yield a relatively wide range in $\delta^{34}S$ values from +22.3 to +26.2‰, with a mean of +24.6±1.6‰; the $\delta^{34}S$ values of light zones range from +25.3 to +27.4‰ (mean of +26.4±0.7‰, n = 8).

The relationship between trace element and $\delta^{34}S$

In Fig. 9, the $\delta^{34}S$ values show a positive correlation with Fe and a negative correlation with Ga, In and Sn when plotted in bulk. However, these correlations cannot be seen when these same data are considered in the context of crystal zonation (Fig. 7). Iron, Co, Ga, In and Sn do not co-vary with the $\delta^{34}S$ values when the geochemical data were plotted from crystal core to rim, which is why the apparent relationships between Fe, Co, Ga, In and Sn and $\delta^{34}S$ on the bulk binary plots is considered meaningful.

Discussion

The relationship between colour and composition

Sphalerite from MVT deposits ranges in colour from white to dark brown with variable yellow to red-brown intermediates. It has been shown that the colours of sphalerite formed in various environments are attributed to the substitution of Fe for Zn in the sphalerite lattice (e.g. Slack *et al.*, 1967; Mclimans *et al.*, 1980; Hill *et al.*, 1985; L'Heureux, 2000; Barrie *et al.*, 2009 and references therein). However, several authors recently found that the colour of colloform sphalerite shows a strong correlation

https://doi.org/10.1180/mgm.2021.29 Published online by Cambridge University Press

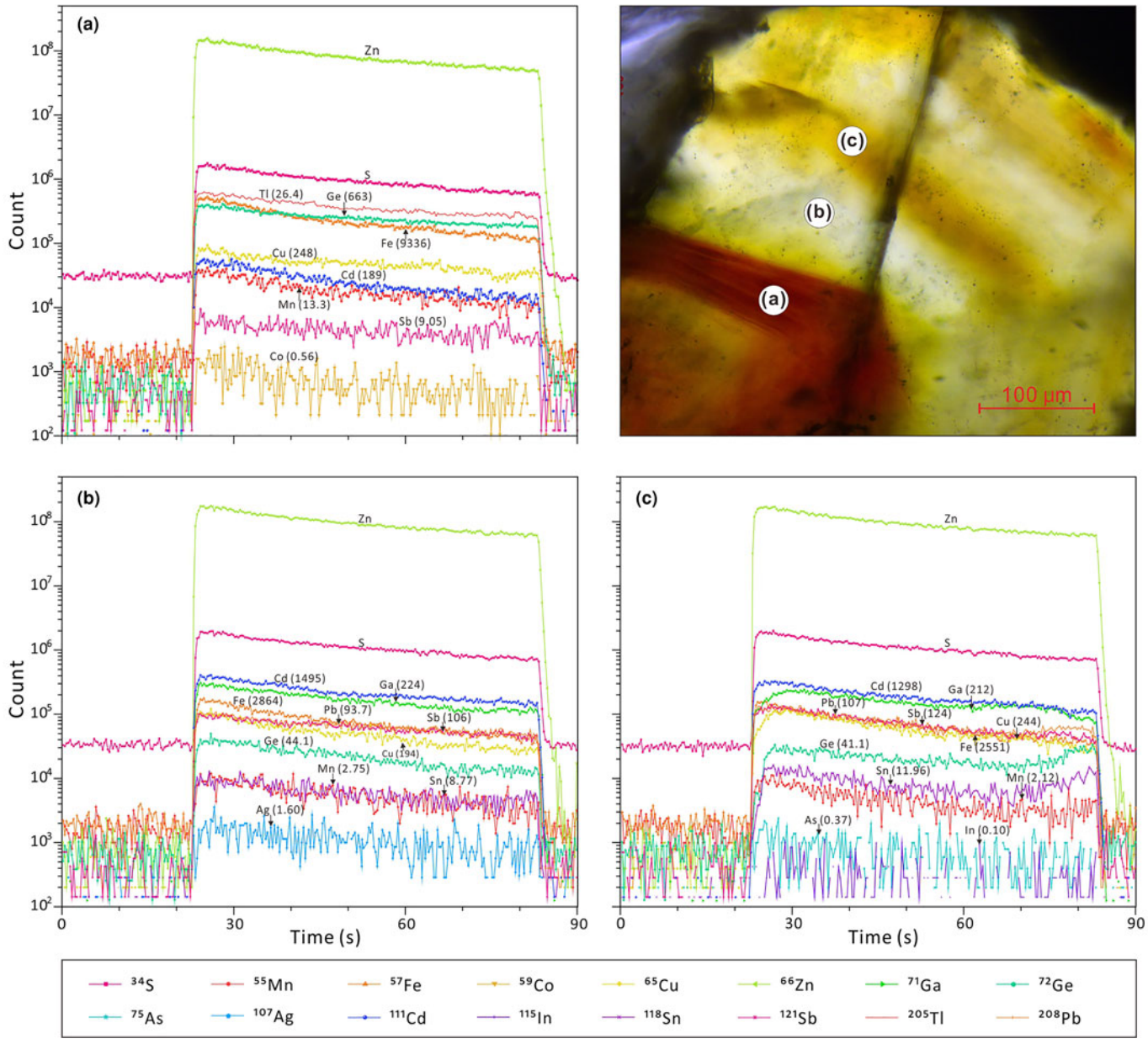

Fig. 3. Typical time-resolved LA-ICP-MS output graphs for the three zoning types, illustrated on a sphalerite crystal (sample 16L-10). (a) Brown cores; (b) pale-yellow zones; and (c) light bands.

with As content rather than Fe content (especially Fe<1.0 wt.%) in studies of MVT deposits (e.g. Pfaff *et al.*, 2011; Gagnevin *et al.*, 2012), leading to the prediction that the crystalline sphalerite at Nayongzhi with higher As concentration tends to be darker. However, the highest As contents (median of 2.08 ppm) were measured in the lightest sphalerite (light bands), suggesting the colour of sphalerite at Nayongzhi is unlikely to be controlled by As concentrations. In contrast, the median value of Fe concentrations increases from 0.20 wt.% in light bands, 0.31 wt.% in pale-yellow zones to 1.14 wt.% in brown cores. This trend suggests sphalerite with higher Fe concentration tends to be darker. In vein-hosted colour-zoned sphalerite of the Dadongla Zn–Hg deposit, South China, elevated Fe concentrations also correlate with brown sphalerite (Hu *et al.*, 2020). Iron has the highest measured concentration in sphalerite compared to any other elements analysed in this investigation and a well-defined correlation between Fe concentration and sphalerite colour was identified. So, the colour in crystallised sphalerite could be tentatively ascribed to Fe variation.

LA-ICP-MS element-distribution maps (Fig. 6) and linear traverses (Fig. 7) display concomitant changes in trace elements, Pb, Ge, Tl and Mn, decrease by an order of magnitude or more from brown cores to light rims. Indium and Co decrease to a lesser extent. Concentrations of Sb, Cd, Ga and Sn increase by an order of magnitude or more at the transition from brown cores to light rims. These elements also show a remarkable correlation with sphalerite colour. However, other studies of zoned sphalerite did not find a correlation between In, Sn, As and Ge and colour (Belissont *et al.*, 2014; Hu *et al.*, 2020). Therefore, the relationship between sphalerite and content of Pb, Ge, Tl, Mn Sb, Cd, Ga and

https://doi.org/10.1180/mgm.2021.29 Published online by Cambridge University Press

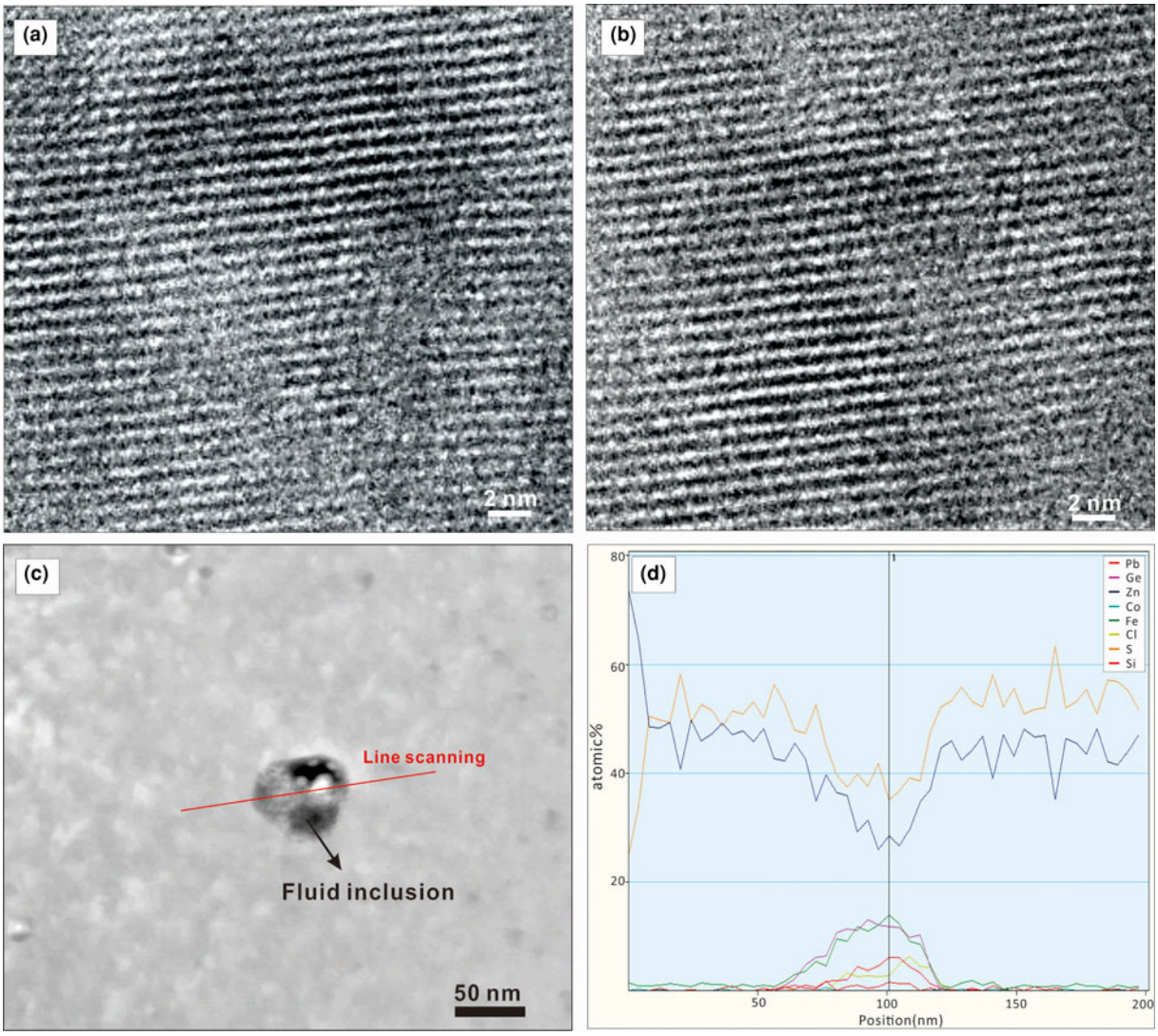

Fig. 4. High-resolution TEM images showing detail of colour zoning in sphalerite: (a) brown core (foil#1); (b) light zone (foil#2); (c) HAADF image showing the fluid inclusions in foil#2 with the red line indicating the position of the EDAX line scan; (d) element concentration distribution along the line scan for Pb, Ge, Zn, Co, Fe, Cl, S and Si.

Sn remains poorly constrained. As many previous studies did not analyse these elements further study is required.

Implications from S isotope composition

Source of sulfur and the precipitation mechanism for sulfides

The *in situ* $\delta^{34}S$ values obtained in this investigation range from +22.3‰ to +27.9‰, which is consistent with previous bulk sulfur isotopic data on the Nayongzhi sphalerite (+17.17‰ to +25.49‰; Fig 8; Jin *et al.*, 2016; Zhou *et al.*, 2018). A plausible explanation for the sulfur compositions of sphalerite is that it is formed by thermochemical sulfate reduction (TSR) of Cambrian marine sulfate (+28‰–+32‰, Claypool *et al.*, 1980). TSR commonly produces sulfur isotope fractionation between SO_4^{2-} and H_2S of 0 to 15‰ (Goldhaber and Kaplan, 1975; Seal, 2006). The lowest $\delta^{34}S$ values observed for sphalerite (+22.3‰) in this study suggests TSR might have occurred alongside the process associated with sulfide precipitation at Nayongzhi, in agreement with previous observations (Jin *et al.*, 2016; Zhou *et al.*, 2018). Overall, the reduced sulfur originates from thermochemical sulfate reduction of seawater sulfate within the ore-hosted strata. It is worth noting that the majority of the metals were derived from the Proterozoic metamorphic basement (e.g. Zhou *et al.*, 2018; Wei *et al.*, 2020). These results suggest metals and reduced sulfur did not travel together in a single hydrothermal fluid, instead a more probable hypothesis is that there is mixing of basement-derived metal-rich fluids and the H_2S-bearing fluid from ore-hosted strata at the site of sulfide precipitation (e.g. Deloule *et al.*, 1986; Pfaff *et al.*, 2010 and references therein), which is in agreement with fluid-inclusion data (Wei, 2018).

Crystal-scale S isotope variations

Considerable S isotope intergrain variations have been observed within individual samples (Table 3 and Fig. 7) and even within single sphalerite grains (up to 4.3‰). To better understand the microscale variation of $\delta^{34}S$ values in Nayongzhi sphalerite, evaluation of the parameters affecting the S isotope compositions is required.

Considering that the reduced sulfur is derived from the same source, other factors, such as temperature, pH, f_{O_2}, and the $\delta^{34}S$

https://doi.org/10.1180/mgm.2021.29 Published online by Cambridge University Press

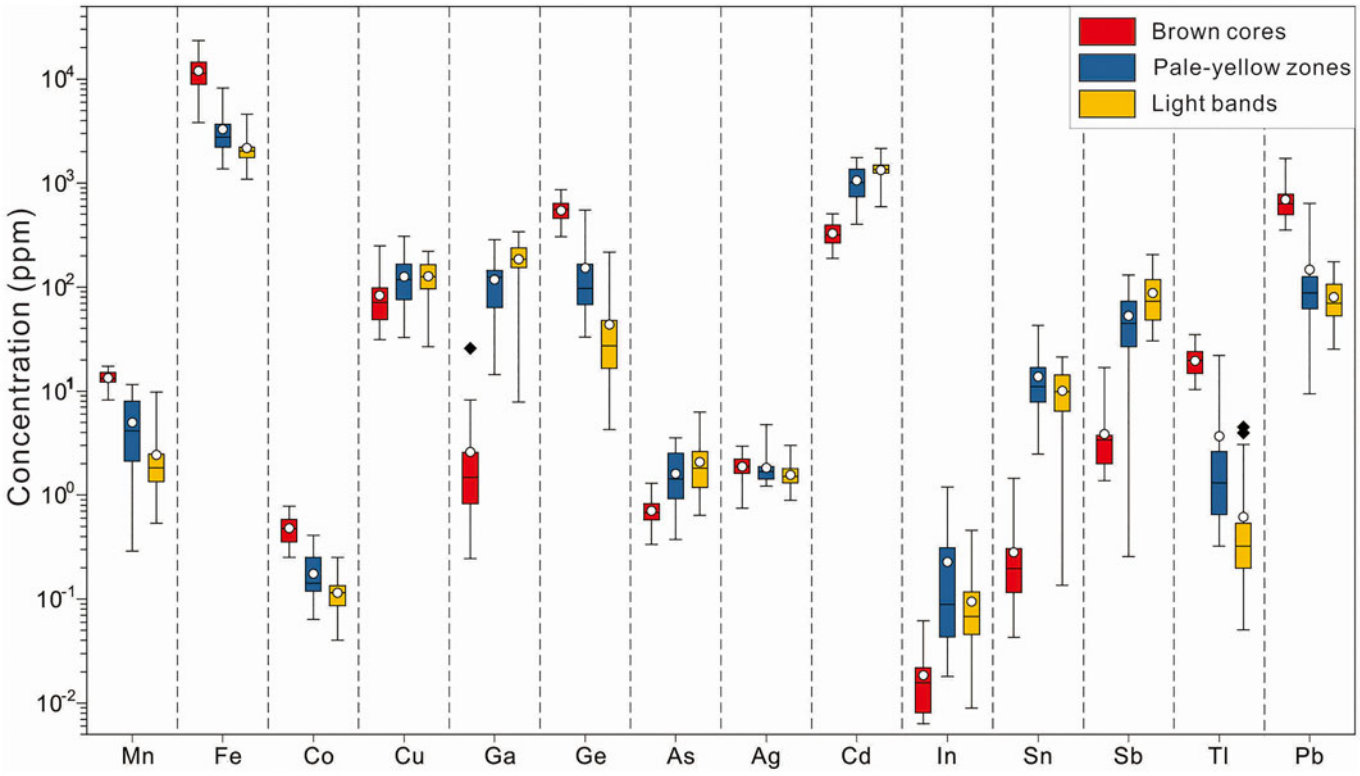

Fig. 5. Boxplots of trace elements in the three identified zoning types within sphalerite from Nayongzhi analysed by LA-ICP-MS. Upper and lower threshold values are 95%. The upper and lower margin of the box represent the upper 75% and 25% of the data. Mean values are shown as solid white circles and median values as solid black lines.

values of the H_2S responsible for precipitating sulfides can significantly influence the S isotope composition of hydrothermal sulfide minerals (Sasaki and Krouse, 1969; Ohmoto, 1972). The fluid-inclusion homogenisation temperature of colour-zoned sphalerite grains ranges from 105.6 to 136.8°C (Table 3 and Fig. 10; data from Wei, 2018), indicating appreciable fluctuations in temperature during the process of sulfide precipitation. However, the S isotopic fractionation between H_2S and ZnS is very small (<1.0‰) in this temperature range. Therefore, temperature cannot be a significant factor in producing the observed $\delta^{34}S$ variation. Calculations presented by Ohmoto (1972) suggest that within the stability field of sphalerite, change in pH, and f_{O_2} would have insignificant influence on $\delta^{34}S$ variation (~0.5‰). Thus, the $\delta^{34}S$ variations in sphalerite appear to have been controlled by predominantly the $\delta^{34}S$ composition of H_2S in the original fluid, although the influence of temperature, pH and/or f_{O_2} cannot be entirely ruled out.

Controls on the zoned sphalerite crystals

Colour bands and/or zones are common in sphalerite in MVT deposits (e.g. Beaudoin, 2000; Barrie *et al.*, 2009). Many studies have proposed two main mechanisms responsible for compositional zoning: (1) internal crystal growth processes representing self-organised phenomena controlled by kinetic factors, such as crystal growth rate and diffusion rate of key elements in the hydrothermal fluid (Fowler and L'Heureux, 1996; Holten *et al.*, 1997; L'Heureux *et al.*, 2000; Benedetto *et al.*, 2005, Belissont *et al.*, 2014); and (2) cyclic variations of external factors (e.g. temperature, f_{O_2}, pH and mineralising fluid composition; Holten *et al.*,1997; Beaudoin, 2000; Kelley *et al.*, 2004; Barrie *et al.*, 2009; Pfaff *et al.*, 2011; Gagnevin *et al.*, 2012 and Hu *et al.*, 2020).

Holten *et al.* (2000) found that the study of neighbouring mineral grains is an effective way to distinguish self-organisation from external fluctuations as the main cause for mineral zoning. It was concluded that, if these minerals grains all show similar zoning, external fluctuations are the probable cause. In Nayongzhi, the colour-zoned sphalerite occurs as a cluster, as shown in Fig. 2b. Wei *et al.* (2018b) found that the hydrothermal dolomite coexisting with colour-zoned sphalerite also displays well-developed colour zoning in cathodoluminescence images. Furthermore, this variation in trace-element composition was observed within single crystals. For instance, concentrations of Fe, Ga, Ge, Sb and Pb vary over two orders of magnitude across different colour zones, suggesting that spontaneous chemical self-organisation is highly unlikely (Figs 5–7). Therefore, the internal crystal processes have a very limited influence on the colour-zoned sphalerite in this investigation. Other factors, such as physicochemical conditions (e.g. pH, temperature and f_{O_2}), mineralising fluid composition and the S isotope variations are probably important (e.g. Kelley *et al.*, 2004; Barrie *et al.*, 2009; Pfaff *et al.*, 2011; Hu *et al.*, 2020 and reference therein).

Physicochemical conditions

It is possible that variation in colour-zoned sphalerite is brought about by changes in the physicochemical conditions accompanying mineralisation (Barton *et al.*, 1977; Pattrick *et al.*, 1993; Pfaff *et al.*, 2011; Gagnevin *et al.*, 2012). Many studies have deduced the pH value fluctuates from 5 to 7 at 150°C for similar MVT Zn–Pb deposits (e.g. Sverjensky, 1984; Leach *et al.*, 2005; Pfaff *et al.*,

https://doi.org/10.1180/mgm.2021.29 Published online by Cambridge University Press

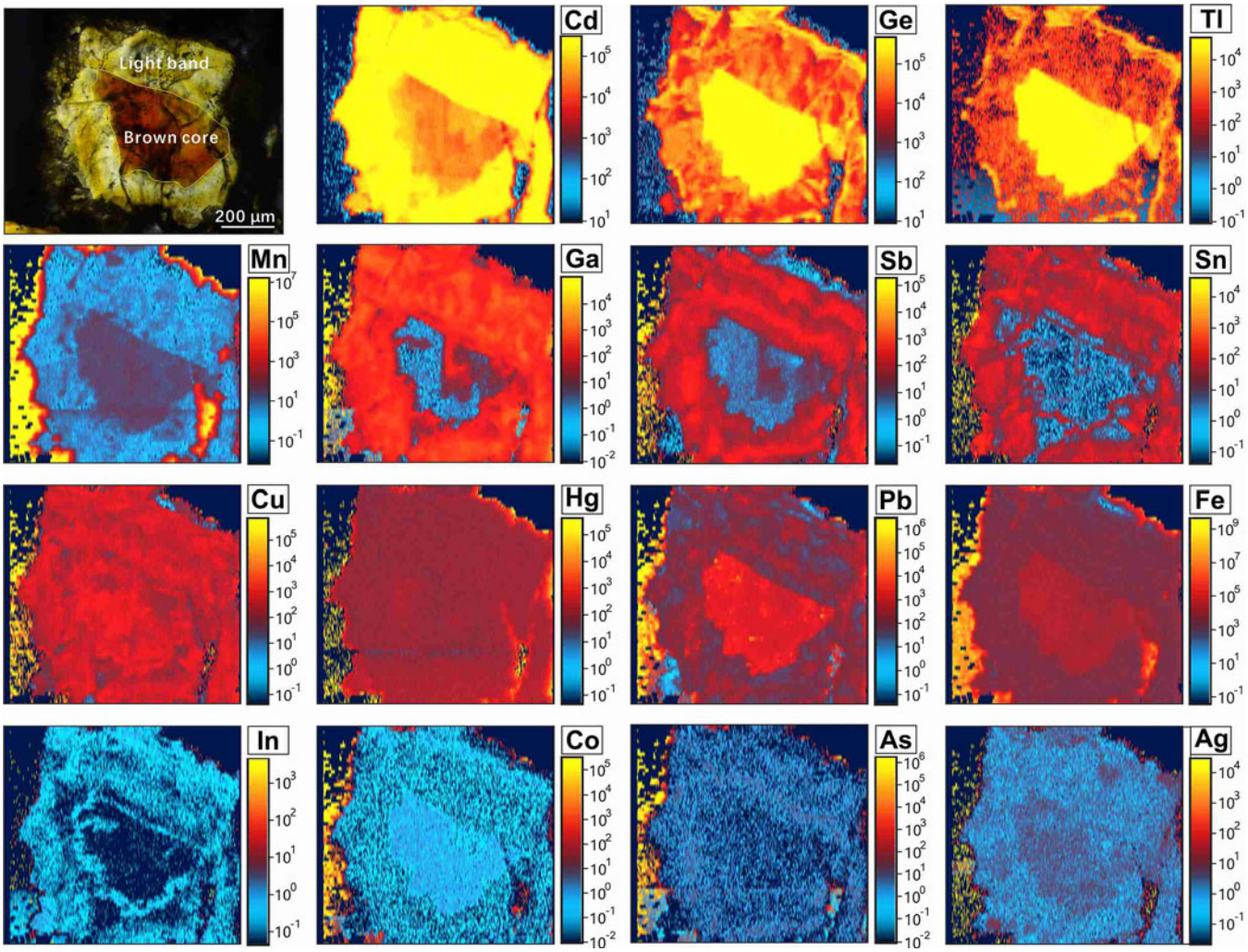

Fig. 6. Elemental maps generated with LA-ICP-MS showing the distribution of selected trace elements in the CR pattern of sphalerite from sample 16S-35.

2010). Redox conditions of the hydrothermal fluids can be estimated qualitatively using the Mn content of sphalerite. Under reduced conditions, Mn tends to be incorporated into sphalerite lattices as MnS rather than forming Mn oxides (Vaughan and Craig, 1997). High Mn concentration in sphalerite thus suggests relatively reduced conditions. At Nayongzhi, the median value of Mn concentrations decreases from brown cores (13.1 ppm), pale-yellow zones (4.32 ppm) to light bands (1.80 ppm), suggesting sphalerite with darker colours tend to be relatively more reduced. There are two pluses in the Mn concentration in the CMR pattern of the sphalerite crystal selected from the proximity of the F_{12} fault. The most pronounced Mn content fluctuation occurs in the first pulse, decreasing from 13.43±0.59 to 1.74±0.45 ppm, and then increasing to 2.53±0.35 ppm. The second pulse is marked by smaller variations (1.94±0.25 ppm–2.87±2.02 ppm). The fluctuation of Mn content indicates the f_{O_2} level experienced at least two pulses during the growth of sphalerite. A similar temperature fluctuation is indicated by Table 3 and Fig. 10. Considering the sulfide precipitation was caused by mixing of two contrasting hydrothermal fluids, the pH showed coordinated variation with these parameters (temperature and f_{O_2}) (Pfaff *et al.*, 2011). In summary, the physicochemical conditions (e.g. pH, temperature and f_{O_2}) are coupled with colour changes during the growth process of the CMR pattern of Nayongzhi sphalerite crystal.

Hydrothermal fluid composition

The distribution of individual metals in sphalerite is also controlled by the composition of ore fluids (e.g. Viets *et al.*, 1992; Kuhlemann and Zeeh, 1995). High Fe, Mn, Ge and Tl contents in brown cores are accompanied by pyrite (Fig. 2c). This would suggest an initial higher concentration of Zn, Fe, Mn and Tl in hydrothermal fluid and a higher sulfidation state relative to other colour bands (the modal volume of minerals decreases in the order: brown sphalerite>pyrite>galena). In contrast, pale-yellow bands of sphalerite are free of mineral inclusions and enriched in In, Sn and Ga, suggesting the fluid responsible for forming the pale-yellow bands has higher concentrations of In, Sn and Ga. Additionally, the relative amounts of Sb and As concentration in light bands and coexisting with high Sb galena (up to 0.35 wt.%; Wei, 2018) infer that the fluid of light zones was elevated in Sb and As. Consequently, the fluid composition also shows a significant influence on the variable trace elements in colour-zoned sphalerite from Nayongzhi.

https://doi.org/10.1180/mgm.2021.29 Published online by Cambridge University Press

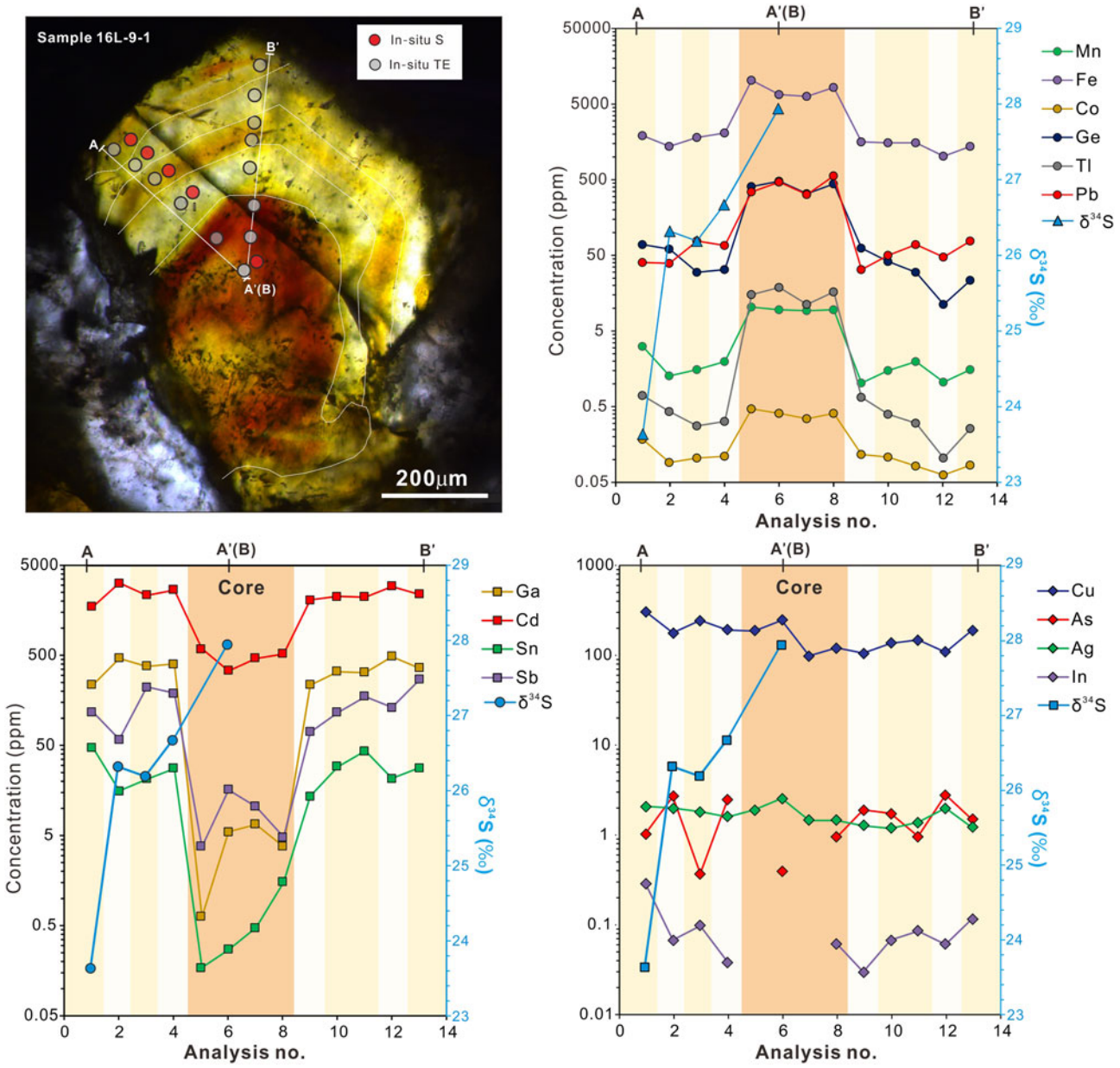

Fig. 7. Detailed traverses obtained for the CMR pattern of sphalerite from sample 16L-9-1 showing the variation of trace elements and sulfur isotopes in a sphalerite crystal. TE= trace elements.

Effect of S isotope variation

The colour-zoned sample shows a clear variation in both colour and S isotope composition from the core to rim (Figs 7–8 and 10). Although colour changes between some zones, especially within the CR texture of the sphalerite crystal do appear to correspond to an associated change in the S isotopic composition, this is not consistent, and the nature of the changes is not systematic between colour zones relative time (from crystal core to rim), which is in agreement with results from other studies (Belissont *et al.*, 2014; Hu *et al.*, 2020). This suggests that the change in sulfur isotopic compositions has no relationship with the colour-zoned sphalerite at Nayongzhi.

In summary, a concomitant change recorded in colour-zoned sphalerite from Nayongzhi has been observed to accompany the changes in physicochemical conditions (e.g. pH, temperature and f_{O_2}) and fluid composition, demonstrating that external factors exert a significant influence on the formation of the zoned sphalerite at Nayongzhi.

Interpretation of the decoupling between $\delta^{34}S$ and trace elements at a crystal scale

We have established that the $\delta^{34}S$ values of zoned sphalerite are controlled mainly by the $\delta^{34}S$ composition of original fluid rather than the change of temperature, pH and/or f_{O_2}. Therefore, the $\delta^{34}S$ variation could not reflect the changes of physicochemical condition during the growth of sphalerite but records the potential source(s) of sulfur. In addition, the significant difference in

https://doi.org/10.1180/mgm.2021.29 Published online by Cambridge University Press

Table 2. *In situ* S isotopic composition for the three colour zones in sphalerite from the Nayongzhi Zn–Pb deposit determined by LA-MC-ICPMS.

Sample no.; colour zoning pattern	Description	Analysis spot	$\delta^{34}S_{V\text{-}CDT}$ (‰)	S.D.
16L-10; CMR	Brown	16L-10Sp1	26.6	0.1
	Pale-yellow	16L-10Sp2	25.9	0.1
	Light	16L-10Sp3	25.8	0.1
	Pale-yellow	16L-10Sp4	24.7	0.1
	Pale-yellow	16L-10Sp5	22.3	0.2
16L-9-1; CMR	Brown	16L-9-1Sp1	27.9	0.1
	Light	16L-9-1Sp2	26.7	0.1
	Pale-yellow	16L-9-1Sp3	26.2	0.1
	Light	16L-9-1Sp4	26.3	0.2
	Pale-yellow	16L-9-1Sp5	23.6	0.1
16S-35; CR	Brown	16S-35Sp1	26.3	0.1
	Light	16S-35Sp2	26.1	0.1
	Brown	16S-35Sp3	27.5	0.1
	Light	16S-35Sp4	25.3	0.1
16S-36; CR	Brown	16S-36Sp1	27.8	0.1
	Light	16S-36Sp2	26.8	0.1
	Brown	16S-36Sp3	27.8	0.1
	Light	16S-36Sp4	27.0	0.1
	Brown	16S-36Sp5	27.9	0.1
	Light	16S-36Sp6	27.4	0.1

S.D. – standard deviation; CMR – core–mantle–rim texture; CR – core–rim texture.

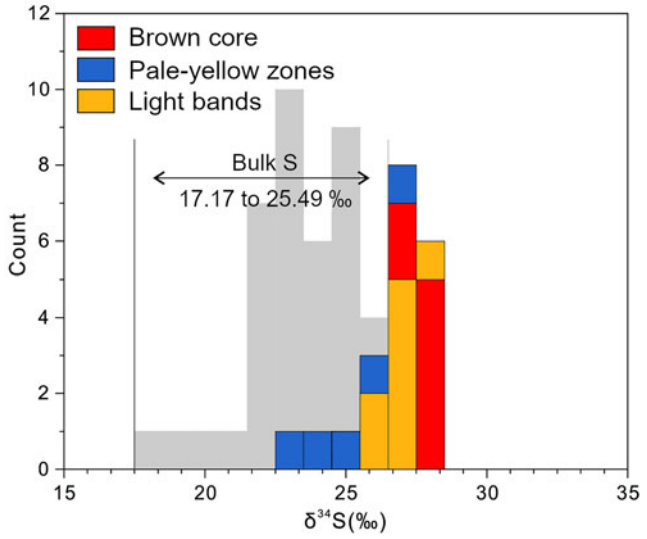

Fig. 8. (a) Histogram of $\delta^{34}S$ variation in the three zones within sphalerite. The bulk S dataset is from Jin *et al.* (2016) and Zhou *et al*. (2018).

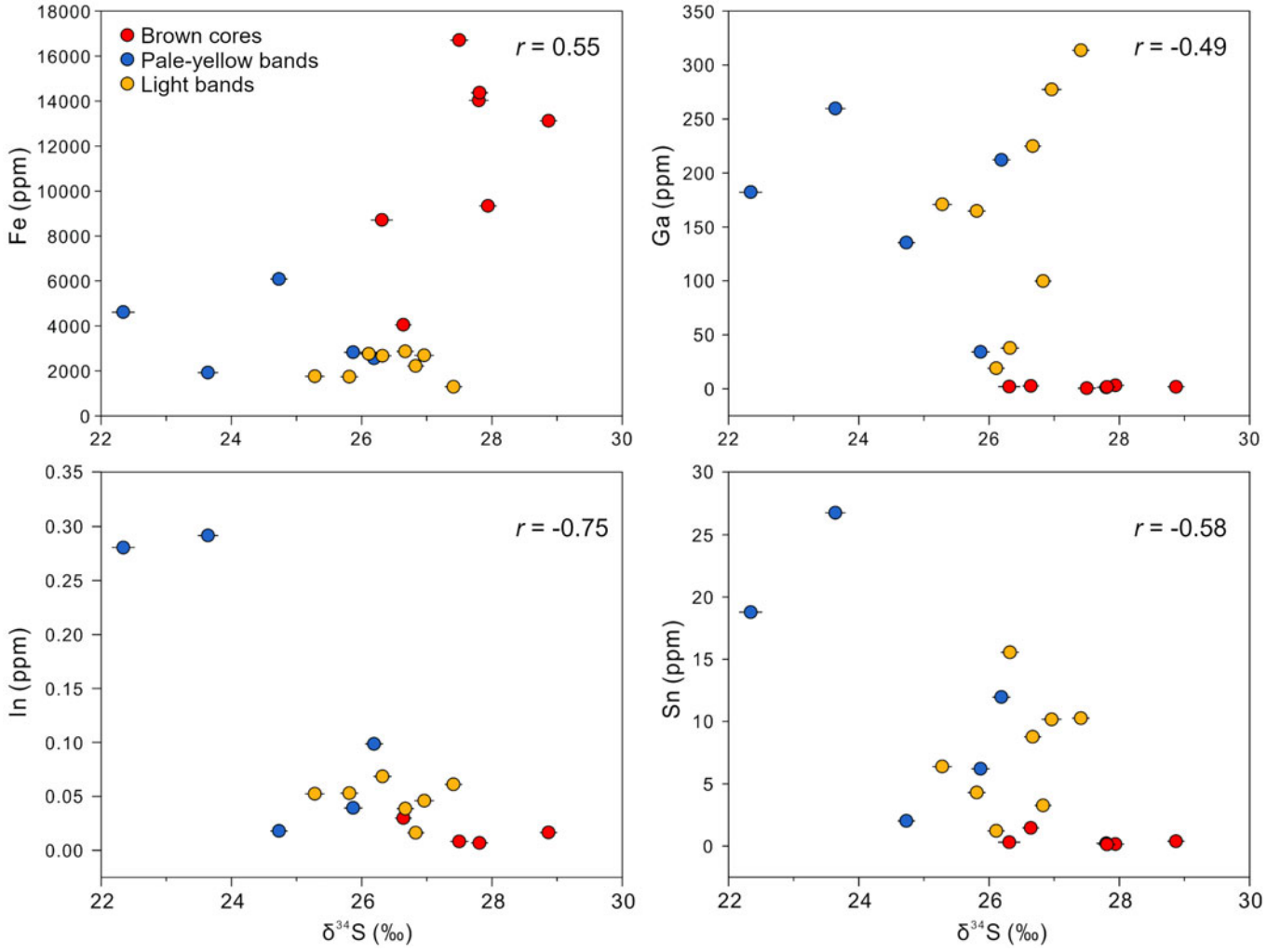

Fig. 9. Binary plots of the Fe, Ga, In and Sn contents of the zoned sphalerite versus $\delta^{34}S$ value.

https://doi.org/10.1180/mgm.2021.29 Published online by Cambridge University Press

Table 3. Microthermometric data for fluid inclusions in the zoned sphalerite sample 16L-9-1 at Nayongzhi.*

Growth stage	Description	Phase description at room temperature	Size (μm)	FI number	Th (°C)	Tm (°C)	Salinity (wt.% NaCl eqv.)
1	Brown Core	L-V, liquid-rich	12×10	1	136.6	−13.3	17.2
1	Brown Core	L-V, liquid-rich	14×8	2	133.8	−12.9	16.8
1	Brown Core	L-V, liquid-rich	16×7	3	133.2	−11.7	15.7
1	Brown Core	L-V, liquid-rich	9×7	4	131.5	−11.1	15.1
Average					133.8	−12.3	16.2
S.D.					2.1	1.0	1.0
2	Light band	L-V, liquid-rich	18×12	1	117.7	−10.5	14.5
2	Light band	L-V, liquid-rich	9×7	2	114.7	−10.3	14.3
2	Light band	L-V, liquid-rich	10×8	3	114.7	−9.2	13.1
2	Light band	L-V, liquid-rich	14×12	4	117.3	−9.5	13.4
2	Light band	L-V, liquid-rich	12×8	5	116.9	−9.3	13.2
Average					116.3	−9.8	13.7
S.D.					1.5	0.6	0.7
3	Pale-yellow	L-V, liquid-rich	24×12	1	124.8	−10.2	14.2
3	Pale-yellow	L-V, liquid-rich	14×11	2	125.3	−10.2	14.2
3	Pale-yellow	L-V, liquid-rich	15×14	3	126.5	−10.4	14.4
3	Pale-yellow	L-V, liquid-rich	12×11	4	123.2	−9.8	13.7
3	Pale-yellow	L-V, liquid-rich	10×9	5	122.5	−10.4	14.4
Average					124.5	−10.2	14.2
S.D.					1.6	0.2	0.3
4	Light band	L-V, liquid-rich	12×11	1	107.9	−7.3	10.9
4	Light band	L-V, liquid-rich	14×8	2	106.2	−6.8	10.2
4	Light band	L-V, liquid-rich	13×8	3	107.2	−8.2	11.9
4	Light band	L-V, liquid-rich	10×9	4	105.6	−8.4	12.2
4	Light band	L-V, liquid-rich	9×8	5	106.4	−8.9	12.7
Average					106.7	−7.9	11.6
S.D.					0.7	0.9	1.0
5	Light band	L-V, liquid-rich	14×9	1	117.3	−8.9	12.7
5	Light band	L-V, liquid-rich	13×12	2	115.6	−8.1	11.8
5	Light band	L-V, liquid-rich	11×10	3	116.2	−8.1	11.8
Average					116.4	−8.4	12.1
S.D.					0.9	0.5	0.5

*Microthermometric data from Wei (2018).
S.D. = Standard Deviation; FI – fluid inclusion; Th – homogenization temperature; Tm – melting temperature.

trace-element concentrations among the three identified colour zones has been recognised. On the basis of the LA-ICP-MS and TEM studies, trace elements commonly occur as solid solutions in colour-zoned sphalerite. We interpret the trace-element variation in sphalerite as a record of external environmental changes (such as pH, temperature, f_{O_2}, and the composition of metal-bearing hydrothermal fluid) during the growth of sphalerite. Systematic changes in metal concentrations in the ore-forming fluid and the physicochemical conditions (e.g. pH, temperature and f_{O_2}) might cause the formation of the colour-zoned sphalerite observed in this investigation. Therefore, all the evidence points to decoupling between $\delta^{34}S$ and trace elements during the formation of the colour-zoned sphalerite at a crystal scale. A plausible explanation is the persistence of a cyclic plumbing system open to the ore solution in Nayongzhi. Episodic injection of ore solution mixes with a reduced sulfur-rich fluid derived from the aquifers of the ore-hosted strata, causing the cyclic changes of pH, temperature, f_{O_2}, and fluid composition and finally forming the colour-zoned sphalerite crystal in Nayongzhi.

Growth history of zoned sphalerite

A pulsed influx of metal-rich fluid was probably significant in the formation of the colour-zoned sphalerite (Fig. 11). In the early stage, deep-seated fluids flowed up the NW-trending F_{12} fault, stalled at the high-porosity Cambrian carbonate rocks, and mixed with the sulfur-rich sedimentary formation water resulting in deposition of the brown sphalerite and/or minor pyrite. During the deposition of the subhedral brown sphalerite, ore fluids were probably reduced as indicated by the high Mn content measured (Fig. 10). Temperature is thought to have been between 131.5°C and 136.6°C on the basis of microthermometry of fluid inclusions within the brown core of the sphalerite (Table 3).

With the deposition of the sulfide ore, the F_{12} fault was sealed, and the original hydrothermal system was restored. As temperature decreases and f_{O_2} increases, Ga, Cd, Sb and As tend to reside in hydrothermal fluid, which mixes with the H_2S-bearing fluid from ore-hosted strata, forming light-coloured zones. After the deposition of light zones, relatively high-temperature basement-derived fluids entered the ore horizon and pale-yellow bands overgrew the pre-existing CR texture of sphalerite in the proximity of the F_{12} fault. Pale-yellow bands could not be observed distal to the F_{12} fault, possibly because of a small volume of basement-derived fluids. Metals carried by the basement-derived hydrothermal fluid are completely precipitated near the F_{12} fault. This interpretation is supported by: (1) the narrow band width (Fig. 2c,d) and the relatively low temperature (122.5–126.5°C) compared to early brown cores (Fig. 10); (2) the decrease of the ore grade and the ore thickness distal to the F_{12} fault (Wei *et al.*, 2020).

https://doi.org/10.1180/mgm.2021.29 Published online by Cambridge University Press

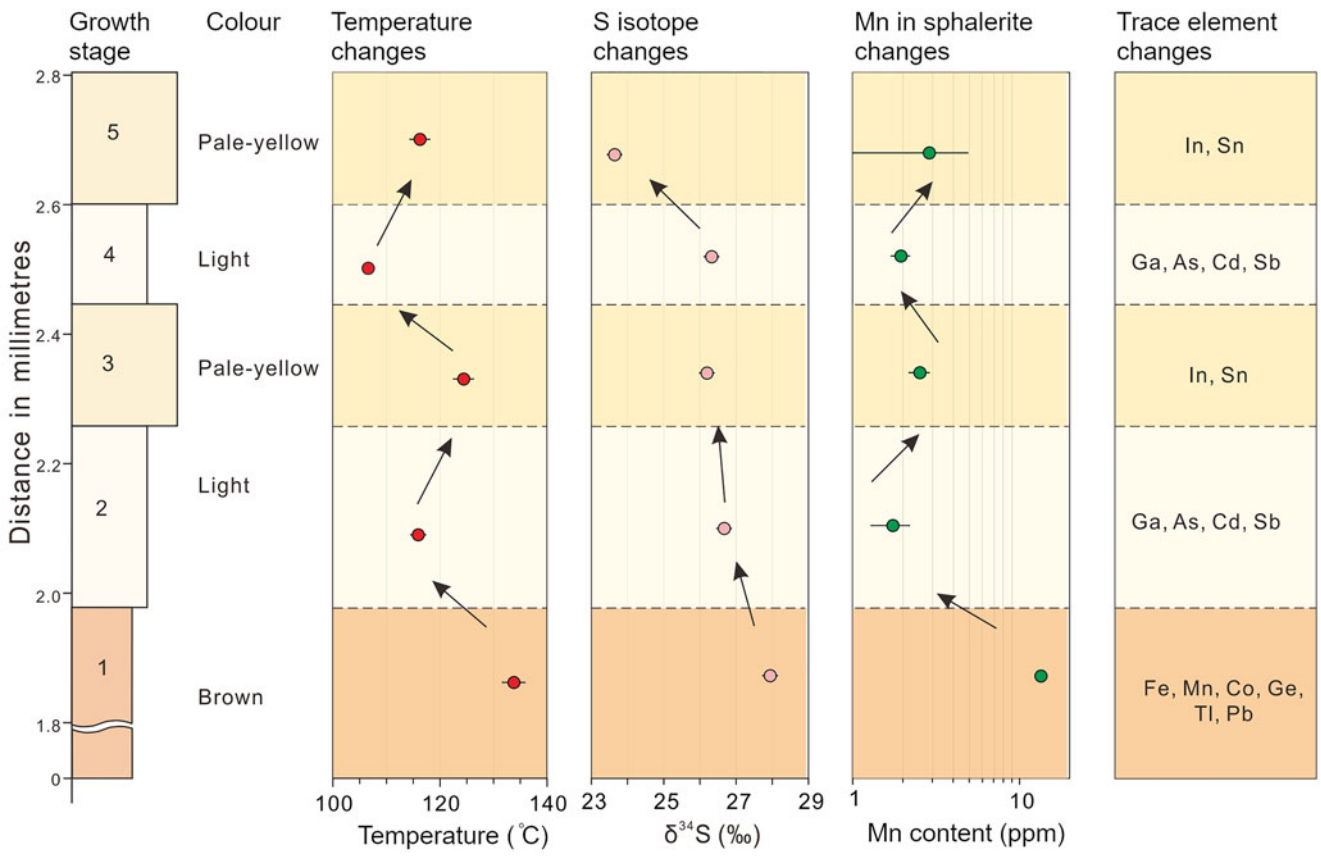

Fig. 10. Diagram correlating changes in colour, S isotope, redox condition, temperature, and trace-element distribution within a typical CMR pattern of the sphalerite sample (16L-9-1) studied.

The cyclic influx of ascending basement-derived fluids caused precipitation of pale-yellow and light zones on pre-existing sphalerite crystals in the proximity of the F_{12} fault, ultimately forming the CMR texture of sphalerite at Nayongzhi.

A similar mechanism has been proposed to explain colour banding within individual sphalerite crystals in the West Shropshire Orefield, England, which is thought to have formed due to episodic injection of hydrothermal fluids that controlled adsorption of various metal cations into zoned sphalerite (Pattrick *et al.*, 1993). Therefore, it is possible that the formation of the colour-zoned sphalerite can be attributed to periodic injection of the ore solution along the same open fracture.

Conclusions and implications

Prior to this investigation, little detailed work had been carried out on the genesis and significance of growth zoning in sphalerite. Microscopic-scale studies of colour-zoned sphalerite have a critical role to play in gaining a better understanding of the growth mechanism of zoned sphalerite. Data obtained by LA-ICP-MS analysis revealed various trace-element compositions in the three identified colour zones. It was found that the sphalerite colour variation could be ascribed tentatively to Fe concentration, due to the relatively lower contents of other metals (Pb, Ge, Tl, Mn Sb, Cd and Ga). Our investigation revealed intracrystalline zonation of $\delta^{34}S$ of up to 4.3‰, which is expected to be controlled by the $\delta^{34}S$ composition of H_2S in the original fluid but the effect of the physicochemical conditions (e.g. temperature, f_{O_2} and pH) cannot be precluded. Poor correlation between trace elements and the $\delta^{34}S$ of colour-zoned sphalerite is ascribed to episodic injection of basement-derived ore solution mixing with a reduced sulfur-rich fluid derived from the aquifers of the ore-hosted strata. During the process, cyclic change of external factors, such as the physicochemical conditions (e.g. temperature and f_{O_2}) and fluid composition cause the formation of the colour-zoned sphalerite crystal at Nayongzhi. Overall, the millimetre and submillimetre scale of compositional variations in the colour-zoned sphalerite suggest the persistence of a cyclic plumbing system open to the ore solution in Nayongzhi, which is responsible for the large compositional range of some trace metals at the micrometre scale.

The use of LA-ICP-MS and TEM to investigate the colour-zoned sphalerite helps to give a better understanding of the occurrence of trace elements in sulfides. The research described here also represents a contribution to revealing the pulse fluid release for the formation of MVT deposits.

https://doi.org/10.1180/mgm.2021.29 Published online by Cambridge University Press

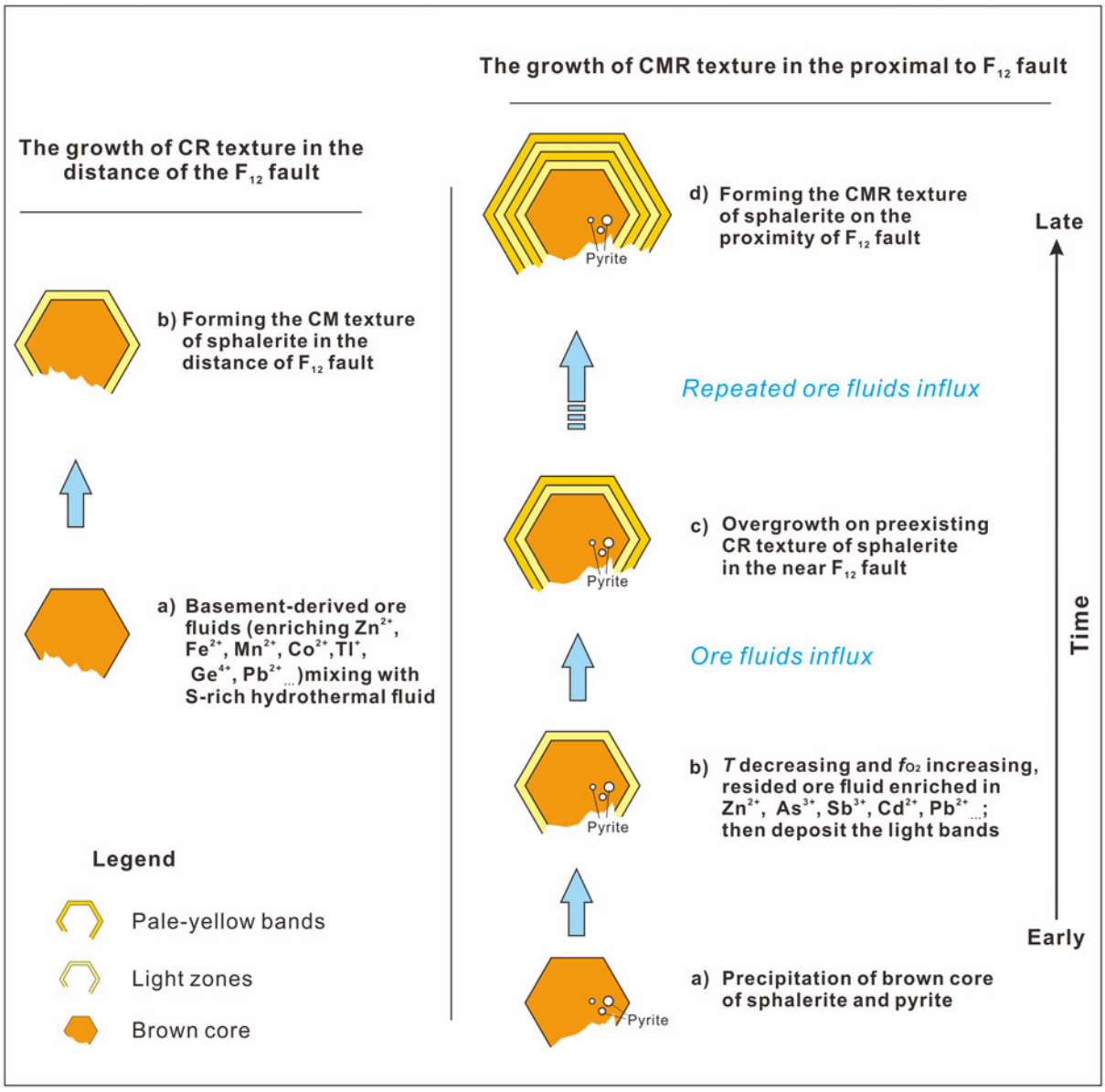

Fig. 11. Schematic diagram showing the growth history of the zoned sphalerite from the Nayongzhi deposit. See text for explanations.

Acknowledgements. This research project was financially supported by the National Natural Science Foundation of China (41673056 and U1812402), the Key Program of Guizhou Natural Science Foundation ([2017]1421) and National Key R&D Program of China (2017YFC0602502). The authors thank Dr. Zhihui Dai at IGCAS and Kaiyun Chen at Northwestern University, China for helping with LA-(MC)-ICP-MS trace elements and sulfur isotopes analyses, respectively. Associate Editor Jason Harvey and two anonymous reviewers are thanked for their constructive comments and suggestions.

Supplementary material. To view supplementary material for this article, please visit https://doi.org/10.1180/mgm.2021.29

References

Barrie C.D., Boyce A.J., Boyle A.P., Williams P.J., Blake K., Wilkinson J.J., Lowther M., McDermott P. and Prior D.J. (2009) On the growth of colloform textures: A case study of sphalerite from the Galmoy orebody, Ireland. *Journal of the Geological Society*, **166**, 563–582.

Barton Jr P.B., Bethke P.M. and Roedder E. (1977) Environment of ore deposition in the Creede Mining district, San Juan Mountains, Colourado: Part III. Progress toward interpretation of the chemistry of the ore-forming fluid for the OH Vein. *Economic Geology*, **72**, 1–24.

Beaudoin G. (2000) Acicular sphalerite enriched in Ag, Sb, and Cu embedded within colour banded sphalerite from the Kokanee Range, BC. *The Canadian Mineralogist*, **38**, 1387–1398.

Belissont R., Boiron M.C., Luais B. and Cathelineau M. (2014) LA-ICP-MS analyses of minor and trace elements and bulk Ge isotopes in zoned Ge-rich sphalerites from the Noailhac-Saint-Salvy deposit (France): insights into incorporation mechanisms and ore deposition processes. *Geochimica et Cosmochimica Acta*, **126**, 518–540.

Chen L., Chen K., Bao Z., Liang P., Sun T. and Yuan H. (2017) Preparation of standards for *in situ* sulfur isotope measurement in sulfides using femtosecond laser ablation MC-ICP-MS. *Journal of Analytical Atomic Spectrometry*, **32**, 107–116.

CIGMR (2003) *Geology map of the Yunnan-Guizhou-Sichuan-Chongqing provinces, scale 1:2,500,000*. Chengdu Institute of Geology and Mineral Resources (CIGMR), China.

Claypool G.E., Holser W.T., Kaplan I.R., Sakai H. and Zak I. (1980) The age curves of sulfur and oxygen isotopes in marine sulfate and their mutual interpretation. *Chemical Geology*, **28**, 199–260.

Cook N.J., Ciobanu C.L., Pring A., Skinner W., Shimizu M., Danyushevsky L., Saini-Eidukat B. and Melcher F. (2009) Trace and minor elements in sphalerite: A LA-ICP-MS study. *Geochimica et Cosmochimica Acta*, **73**, 4761–4791.

Cook N.J., Sundblad K., Valkama M., Nygård R., Ciobanu C.L. and Danyushevsky L. (2011) Indium mineralisation in A-type granites in south-eastern Finland: insights into mineralogy and partitioning between coexisting minerals. *Chemical Geology*, **284**, 62–73.

Danyushevsky L., Robinson P., Gilbert S., Norman M., Large R., McGoldrick P. and Shelley M. (2011) Routine quantitative multi-element analysis of sulphide minerals by laser ablation ICP-MS: standard development and consideration of matrix effects. *Geochemistry: Exploration, Environment, Analysis*, **11**, 51–60.

Deloule E., Allegre C., Doe B. (1986) Lead and sulfur isotope microstratigraphy in galena crystals from Mississippi Valley-type Deposits. *Economic Geology*, **81**, 1307–1321

Di Benedetto F., Bernardini G.P., Costagliola P., Plant D. and Vaughan D.J. (2005) Compositional zoning in sphalerite crystals. *American Mineralogist*, **90**, 1384–1392.

Fowler D.A. and L'Heureux I. (1996) Self-organized banded sphalerite and branching galena in the Pine Point ore deposit, Northwest Territories. *The Canadian Mineralogist*, **34**, 1211–1222

Frenzel M., Mikolajczak C., Reute M.A. and Gutzmer J. (2017) Quantifying the relative availability of high-tech by-product metals–the cases of gallium, germanium and indium. *Resource Policy*, **52**, 327–335

Gagnevin D., Menuge J. F., Kronz A., Barrie C. and Boyce A.J. (2012) Minor elements in layered sphalerite as a record of fluid origin, mixing, and crystallisation in the Navan Zn–Pb ore deposit, Ireland. *Economic Geology*, **109**, 1513–1528.

Goldhaber M. B. and Kaplan I. R. (1975) Controls and consequences of sulfate reduction rates in recent marine sediments. *Soil Science*, **119**, 42–55.

Hill G. S., Rowlands N. and Finch J. (1985) Correlation between colour and iron content in Pine Point sphalerites. *Economic Geology*, **80**, 2035–2037.

Höll R., Kling M. and Schroll E. (2007) Metallogenesis of germanium – a review. *Ore Geology Reviews*, **30**, 145–180.

Holten T., Jamtveit B., Meakin P., Cortini M., Blundy J. and Austrheim H. (1997) Statistical characteristics and origin of oscillatory zoning in crystals. *American Mineralogist*, **82**, 596–606

Holten T., Jamtveit B. and Meakin P. (2000) Noise and oscillatory zoning of minerals. *Geochimica et Cosmochimica Acta*, **11**, 1893–1904.

Hu Y. S., Ye L., Wei C., Li Z. L Huang Z. L. and Wang H. Y. (2020) Trace Elements in Sphalerite from the Dadongla Zn–Pb Deposit, Western Hunan–Eastern Guizhou Zn–Pb Metallogenic Belt, South China. *Acta Geologica Sinica* (English Edition), **94**, 2152–2164

Jin Z.G., Zhou J.X., Huang Z.L., Luo K., Gao J.G., Peng S., Wang B. and Chen X.L. (2016) Ore genesis of the Nayongzhi Pb-Zn deposit, Puding city, Guizhou Province, China: Evidences from S and *in situ* Pb isotopes. *Acta Petrologica Sinica*, **32**, 3441–3455 [in Chinese with English Abstract].

Kelley K.D., Leach D.L., Johnson C.A., Clark J.L., Fayek M., Slack J.F., Anderson V.M., Ayuso R.A. and Ridley W.I. (2004) Textural, compositional, and sulfur isotope variations of sulfide minerals in the Red Dog Zn–Pb-Ag deposits, Brooks Range, Alaska: Implications for ore formation. *Economic Geology*, **99**, 1509–1532

Kuhlemann J. and Zeeh S. (1995) Sphalerite stratigraphy and trace element composition of east Alpine Pb-Zn deposits (Drau Range, Austria-Slovenia). *Economic Geology*, **90**, 2073–2080.

Large R.R., Danyushevsky L., Hollit C., Maslennikov V., Meffre S., Gilbert S., Bull S., Scott R., Embsbo P., Thomas H., Singh B. and Foster J. (2009) Gold and trace element zonation in pyrite using a laser imaging technique: Implications for the timing of gold in orogenic and Carlin style sediment-hosted deposits. *Economic Geology*, **104**, 635–668.

Leach D.L., Sangster D., Kelley K.D., Large R.R., Garven G., Allen C., Gutzmer J. and Walters S. (2005) Sediment-hosted lead-zinc deposits: A global perspective. *Economic Geology 100th Anniversary*, 561–607.

L'Heureux I. (2000) Origin of banded patterns in natural sphalerite. *Physical Review,* **E62**, 3234–3245.

Longerich H.P., Jackson S.E. and Gunther D. (1996) Laser ablation inductively coupled plasma mass spectrometric transient signal data acquisition and analyte concentration calculation. *Journal of Analytical Atomic Spectrometry*, **11**, 899–904.

McLimans R.K., Barnes H.L. and Ohmoto H. (1980) Sphalerite stratigraphy of the upper Mississippi Valley zinc-lead district, southwest Wisconsin. *Economic Geology*, **75**, 351–361.

Ohmoto H. (1972) Systematics of sulfur and carbon isotopes in hydrothermal ore deposits. *Economic Geology*, **67**, 551–578.

Paton C., Hellstrom J., Paul B., Woodhead. J. and Hergt J. (2011) Iolite: Freeware for the visualisation and processing of mass spectrometric data. *Journal of Analytical Atomic Spectrometry*, **26**, 2508–2518.

Pattrick R.A.D., Dorling M. and Polya D.A. (1993) TEM study of indium bearing and copper-bearing growth-banded sphalerite. *The Canadian Mineralogist*, **31**, 105–117.

Pfaff K., Hildebrandt L.H., Leach D.L., Jacob D.E. and Markl G. (2010) Formation of the Wiesloch Mississippi Valley-type Zn–Pb–Ag deposit in the extensional setting of the Upper Rhinegraben, SW Germany. *Mineralium Deposita*, **45**, 647–666.

Pfaff K., Koenig A., Wenzel T., Ridley I., Hildebrandt L.H., Leach D.L. and Markl G. (2011) Trace and minor element variations and sulfur isotopes in crystalline and colloform ZnS: Incorporation mechanisms and implications for their genesis. *Chemical Geology*, **286**, 118–134.

Roedder E. (1968). Noncolloidal origin of colloform textures in sphalerite ores. *Economic Geology*, **63**, 451–471.

Roedder E. and Dwornik E.J. (1968). Sphalerite colour banding: Lack of correlation with iron content, Pine Point, Northwest Territories, Canada. *American Mineralogist*, **53**, 1523–1529.

Sasaki A. and Krouse H.R. (1969) Sulfur isotopes and the Pine Point lead–zinc mineralization. *Economic Geology*, **64**, 718–730.

Seal I.R. (2006) Sulfur isotope geochemistry of sulfide minerals. Pp. 633–677 in: *Sulfide Mineralogy and Geochemistry* (D.J. Vaughan, editor). Reviews in Mineralogy and Geochemistry, **61**. Mineralogical Society of America and the Geochemical Society, Chantilly, Virginia, USA.

Slack G.A., Roberts S., Ham F.S. (1967) Far-infrared optical absorption of Fe^{2+} in ZnS. *Physical Reviews*, **155**, 170–177.

Sverjensky D.A. (1984) Oil field brines as ore-forming solutions. *Economic Geology*, **79**, 23–37.

Vaughan D.J. and Craig J.R. (1997) Sulfide mineral stabilities, morphologies, and intergrowth texture. Pp. 367–434 in: *Geochemistry of Hydrothermal Ore Deposits—Third Edition* (H.L. Barnes, editor). John Wiley, New York.

Viets J.G., Hopkins R.T. and Miller B.M. (1992) Variations in minor and trace-metals in sphalerite from Mississippi Valley-type deposits of the Ozark Region: Genetic implications. *Economic Geology*, **87**, 1897–1905.

Wei C. (2018) *Ore-Forming Fluid and Ore Genesis of The Nayongzhi Deposit in Northwestern Guizhou, China*. A Thesis Submitted to University of Chinese Academy of Sciences, 106 pp [in Chinese with English abstract].

Wei C., Huang ZL., Yan Z.F., Hu Y.S. and Ye L. (2018a) Trace element contents in Sphalerite from the Nayongzhi Zn–Pb deposit, Northwestern Guizhou, China: Insights into incorporation mechanisms, metallogenic temperature and ore genesis. *Minerals*, **8**, 490.

Wei C., Yan Z.F., Huang Z.L. and Hu Y.S. (2018b) Geochemical characteristics of the hydrothermal dolomite from the Nayongzhi deposit, Northwestern Guizhou, China and their prospecting indication. *Acta Mineralogica Sinica*, **38**, 666–674 [in Chinese with English abstract].

Wei C., Ye L., Huang Z.L., Hu Y.S. and Wang H.Y. (2020) New advances in the study of Pb-Zn deposits in the Wuzhishan district of northwest Guizhou: Enlightenment on the attribution of metallogenic belt. *Acta Mineralogica Sinica*, **40**, 394–403 [in Chinese with English abstract].

Zhou J.X., Wang X.C., Wilde S.A., Luo K., Huang Z.L., Wu T. and Jin Z.G. (2018) New insights into the metallogeny of MVT Zn–Pb deposits: A case study from the Nayongzhi in South China, using field data, fluid compositions, and *in situ* S-Pb isotopes. *American Mineralogist*, **103**, 91–108.

https://doi.org/10.1180/mgm.2021.29 Published online by Cambridge University Press